Dependence of the dynamic moduli of heterogeneous nematic polymers on planar anchoring relative to flow direction

Eric P. Choate
Department of Applied Mathematics,
Naval Postgraduate School
Monterey, CA 93943

M. Gregory Forest
Department of Mathematics,
Institute for Advanced Materials
University of North Carolina at Chapel Hill
Chapel Hill, NC 27599-3250

May 6, 2011

Abstract

We analyze the dynamic moduli of nematic polymers in a parallel plate oscillatory shear experiment from a Doi-Marrucci-Greco orientation tensor formulation, paying special attention to the inherent connection between rheological properties and wall anchoring conditions. We assume standard experimental procedures in which the plates have been rubbed to achieve strong nematic anchoring parallel to the rubbing direction. We derive the heterogeneous, harmonic response of the nematic liquid in the weak oscillatory shear regime of linear viscoelasticity. The response function is parameterized by the orientational anchoring condition, and in particular by the angle of rotation between the rubbing direction and the flow direction. From this analysis, we read off the frequency-dependent storage and loss moduli. The dominant effect is in the storage modulus where for high frequencies rubbing aligned with the vorticity axis can cause G' to be two-to-three orders of magnitude larger than rubbing in the flow direction. This anchoring dependency shows the significance of the order parameter fluctuations of tensor-based models: Leslie-Ericksen theory predicts zero storage modulus for vorticity-aligned anchoring. For low frequencies, this effect is reversed with flow-aligned anchoring maximizing G' in a manner similar to Leslie-Ericksen theory although we predict a nonzero modulus for vorticity-aligned anchoring.

1 Introduction

The orientational equilibria of a nematic liquid crystal polymer (Brownian rods in a viscous solvent) are degenerate in the absence of an external field. Factors such as rod concentration and aspect ratio determine the equilibrium degree of ordering (a uniaxial equilibrium order parameter we denote by s_0). However, external forces such as electromagnetic fields, fluid flow, or anchoring conditions at a solid boundary select the major director $\mathbf{n}_1$, the preferred direction of this orientational alignment distribution. Boundary anchoring conditions have been shown experimentally to affect the rheological properties of the system [Mendil et al., 2005, 2006; Pujolle-Robic and Noirez, 2001; Holmes et al., 2010].

In this paper, we continue our analytical studies of the sensitivity of the dynamic moduli of nematic liquid crystal polymers due to tunable orientational anchoring conditions at solid boundaries [Choate et al., 2008, 2010]. We consider a parallel plate shear cell where the two plates have been mechanically rubbed to induce uniaxial equilibrium anchoring with the major director parallel to the direction of the rubbing. The entire sample then assumes this homogeneous equilibrium. This allows a study of the viscoelastic response to small amplitude oscillatory shear, where we focus on the dependence of the moduli on the angle θ_0 between the shearing plane and the anchoring major director, which we parameterize as

$$\mathbf{n}_0 = (\cos\theta_0, 0, \sin\theta_0)^T. \tag{1}$$

There are two distinct response modes that one can anticipate in these oscillatory shear experiments. One orientational response is director dominated: The major director $\mathbf{n}_1$ oscillates about its equilibrium orientation while the shape of the distribution, as measured by the order parameters, remains essentially constant. Another response mode is dominated by fluctuations of the degrees of orientation about a relatively constant major director. Leslie-Ericksen (LE) theory is limited to the first shear response mode. Doi-Marrucci-Greco (DMG) and Landau-de Gennes tensor models capture both response modes, and perhaps more importantly, the tensor model solutions offer the ability to discern the relative contributions to dynamic moduli from the director versus order parameter oscillations. This perspective is carried out here for the DMG tensor model, and the results are compared versus the angle between the plate motion and anchoring angle. In this study, we find a continuous transition between these two modes of a tensor model by tuning only the angle θ_0 between the rubbing direction and the flow direction.

The two limiting values of θ_0 are noteworthy. When $\theta_0 = 0$, the anchoring director lies in the flow-flow gradient plane. Due to the symmetry of the system with respect to this plane, the full five-dimensional system for the symmetric, trace-1 second moment tensor $\mathbf{M}$ reduces to a three-dimensional subspace when the major director starts "in-plane." The authors have previously examined this "flow-aligned" anchoring case [Choate et al., 2008, 2010] and found that the tensor models adhere to the first behavior mode (director-dominated or LE-like) when the major director is aligned parallel to the flow direction. The order parameters are constant at leading order.

The other extreme anchoring condition corresponds to $\theta_0 = \frac{\pi}{2}$, in which the major director is aligned parallel to the vorticity axis in a manner similar to the "logrolling" orientation seen in some steady shear experiments. The LE equations are trivially satisfied by the constant major director $\mathbf{n}(y,t) \equiv (0,0,1)^T$, so this model cannot allow perturbations from

the equilibrium state for vorticity-aligned anchoring. This predicts purely viscous behavior of the fluid. However, from the tensor model standpoint, vorticity-aligned anchoring pins the eigenvector of $\mathbf{M}$ corresponding to its unique largest eigenvalue to be parallel to the vorticity axis, which effectively reduces the system to a three-dimensional subspace not unlike the flow-aligned anchoring case. There is one degree of freedom for the pair of eigenvectors confined to the shearing plane, but this effect does not contribute at leading order. Thus, the significant dynamics in the vorticity-aligned system are confined to the order parameters, which provides features that the LE model cannot predict.

For values of θ_0 in between these two extremes, we can solve the system numerically and make predictions of the dynamic moduli. These predictions can be effectively modeled as a superposition of a monodomain prediction, which is dominated by the order parameter perturbations, and an LE-like prediction, which has only director perturbations.

We observe two different regimes of behavior of the storage modulus based on frequency. For a fixed high frequency ω, G' increases monotonically with θ_0, and vorticity-aligned anchoring yields a two-to-three orders of magnitude larger modulus than flow-aligned. This stands in contrast to LE theory, which predicts that G' decreases with θ_0. However, for a fixed low frequency, vorticity-aligned anchoring minimizes G', but the variations due to θ_0 are only factors of two-to-three as opposed to order of magnitude, which is consistent with LE predictions.

The loss modulus $G''(\omega)$ is very nearly linear with ω, and so it is easier to analyze the dynamic viscosity $\eta' = \frac{G''(\omega)}{\omega}$. The viscosity is maximized when the major director is aligned in the shearing plane and minimized by vorticity-aligned anchoring, decreasing monotonically with θ_0 for each fixed frequency. There is negligible frequency dependence for $\theta_0 = 0$, whereas for $\theta_0 = \frac{\pi}{2}$, the high frequency response is five-to-ten percent less viscous than the low frequency response.

These effects can be captured quite nicely by a linear superposition of two simpler analytical models. A monodomain model emphasizes the order parameter contributions, and it predicts a storage modulus that increases with θ_0. A Leslie-Ericksen-like model allows only major director variations and predicts a storage modulus with decreases with θ_0. Taken together, these two effects can explain the transition between the high and low frequency regimes in the dynamic moduli.

2 Model formulation and dimensional analysis

We use the same nondimensionalization as our previous studies [Choate et al., 2008, 2010] in order to make a connection with LE studies [de Andrade Lima and Rey, 2004, 2006; Burghardt, 1991]. The characteristic Frank stress is $\tau_F = \frac{K}{h^2} = \frac{\nu k T N \mathcal{L}^2 s_0^2}{8h^2}$, and the characteristic Leslie viscosity is $\eta_0 = \frac{\nu k T s_0^2}{D_r}$, for the Frank elasticity constant K, the polymer number density ν, the Boltzmann constant k, the temperature T, the penetration depth $\mathcal{L}$ of the elasticity potential, the rotational diffusion rate D_r, and the characteristic length h, which is gap width of our parallel plate shear cell. The equilibrium order parameter is $s_0 = \frac{1}{4}(1 + 3\sqrt{1 - \frac{8}{3N}})$, where N is the dimensionless strength of the excluded volume potential. The characteristic timescale is $t_0 = \frac{\eta_0}{\tau_F} = \frac{8h^2}{N\mathcal{L}^2 D_r}$.

As in [Choate et al., 2008, 2010], the solutions from imposed stress boundary conditions are equivalent to those with imposed velocity boundary conditions up to a rescaling and a phase shift. By virtue of this correspondence principle, we choose to impose the nondimensional velocity boundary conditions $v_x(y=\pm\frac{1}{2},t)=\pm Er\cos\omega t$, where the Ericksen number $Er=\frac{\dot\gamma_0\eta_0}{\tau_F}$ is the ratio of the effective flow-induced viscous boundary stress $\dot\gamma_0\eta_0$ to the Frank stress. The Deborah number $De=\frac{\dot\gamma_0}{D_r}$ is the ratio of the shear rate $\dot\gamma_0$ to the rotational diffusion rate. Their ratio is

$$\alpha=\frac{Er}{De}=\frac{\eta_0 D_r}{\tau_F}=\frac{t_0}{D_r^{-1}}=\frac{8h^2}{N\mathcal{L}^2}. \tag{2}$$

While the Ericksen number measures the strength of distortional stress relative to the applied stress at the boundary, α represents the relative strengths of the excluded volume potential and the distortional elasticity potential, which extends the anchoring conditions into the interior of the domain independently of the driving conditions. It is therefore a property of the material in a confined space and not the flow.

The nondimensional evolution equation for the second moment tensor $\mathbf{M}$ of the orientational probability density function f is

$$\begin{aligned}\tfrac{D}{Dt}\mathbf{M}=\;&\boldsymbol{\Omega}\cdot\mathbf{M}-\mathbf{M}\cdot\boldsymbol{\Omega}+a(\mathbf{D}\cdot\mathbf{M}+\mathbf{M}\cdot\mathbf{D}-2\mathbf{D}:\mathbf{M}_4)\\&-6\,\alpha[\mathbf{Q}-N(\mathbf{M}\cdot\mathbf{M}-\mathbf{M}:\mathbf{M}_4)]+\Delta\mathbf{M}\cdot\mathbf{M}+\mathbf{M}\cdot\Delta\mathbf{M}-2\Delta\mathbf{M}:\mathbf{M}_4,\end{aligned} \tag{3}$$

where $\mathbf{Q}=\mathbf{M}-\frac{\mathbf{I}}{3}$ and $\mathbf{M}_4$ is the fourth moment of f, which we approximate by $\mathbf{M}_4\approx\mathbf{MM}$ to close the system on $\mathbf{M}$ and $\mathbf{v}$. The molecular shape parameter is $a=\frac{R^2-1}{R^2+1}$, for the aspect ratio R of the spheroidal molecules. We assume the velocity takes the form $\mathbf{v}=(v_x(y),0,0)^T$, and it enters the equations through the vorticity tensor $\boldsymbol{\Omega}=\frac{1}{2}(\nabla\mathbf{v}-\nabla\mathbf{v}^T)$ and rate-of-strain tensor $\mathbf{D}=\frac{1}{2}(\nabla\mathbf{v}+\nabla\mathbf{v}^T)$. The nondimensional stress tensor is

$$\begin{aligned}\boldsymbol{\tau}=\;&\tfrac{3a\alpha}{s_0^2}[\mathbf{Q}-N(\mathbf{M}\cdot\mathbf{M}-\mathbf{M}:\mathbf{M}_4)]+\tfrac{1-a}{2s_0^2}\mathbf{M}\cdot\Delta\mathbf{M}-\tfrac{1+a}{2s_0^2}\Delta\mathbf{M}\cdot\mathbf{M}+\tfrac{a}{s_0^2}\Delta\mathbf{M}:\mathbf{M}_4\\&-\tfrac{1}{4s_0^2}(M_{kl,i}M_{kl,j}-\mathbf{M}:\nabla\nabla\mathbf{M})+\mu_1(\mathbf{D}\cdot\mathbf{M}+\mathbf{M}\cdot\mathbf{D})+\mu_2\mathbf{D}:\mathbf{M}_4+\mu_3\mathbf{D},\end{aligned} \tag{4}$$

where μ_i are dimensionless molecular-shape-dependent viscosities [Wang, 2002]. As in [Choate et al., 2008, 2010], the Reynolds number $Re=\frac{\rho h^2}{\tau_F t_0^2}$ is quite small, and so we use the Stokes limit in the linear momentum balance, $\nabla\cdot\boldsymbol{\tau}=\mathbf{0}$.

It is common to express the five degrees of freedom of the second moment tensor with the spectral representation $\mathbf{M}=s(\mathbf{n}_1\mathbf{n}_1-\frac{\mathbf{I}}{3})+\beta(\mathbf{n}_2\mathbf{n}_2-\frac{\mathbf{I}}{3})+\frac{\mathbf{I}}{3}$, where the order parameters $s=d_1-d_3$ and $\beta=d_2-d_3$ represent the differences of the eigenvalues d_i of $\mathbf{M}$. The director angles θ, ψ, and χ parameterize the corresponding eigenvectors as $\mathbf{n}_1=(\cos\theta\cos\psi,\cos\theta\sin\psi,\sin\theta)^T$, $\mathbf{n}_2=(-\sin\theta\cos\psi\sin\chi-\sin\psi\cos\chi,-\sin\theta\sin\psi\sin\chi+\cos\psi\cos\chi,\cos\theta\sin\chi)^T$, and $\mathbf{n}_3=\mathbf{n}_1\times\mathbf{n}_2$. The in-plane subspace corresponds to $\theta=\chi=0$, leaving ψ as the in-plane director angle. However, in this paper, we wish to examine the vorticity-aligned case $\theta=\frac{\pi}{2}$, which causes this spectral representation to become degenerate. Therefore, we will examine the system for the components $M_{11}, M_{22}, M_{12}, M_{13}$, and M_{23} directly.

The uniaxial nematic equilibrium anchoring conditions with major director (1) translate to the second moment tensor anchoring condition

$$\mathbf{M}(y=\pm\frac{1}{2})=\mathbf{M}_0=s_0(\mathbf{n}_0\mathbf{n}_0-\frac{\mathbf{I}}{3})+\frac{\mathbf{I}}{3}=s_0\begin{bmatrix}\cos^2\theta_0-\frac{1}{3} & 0 & \frac{1}{2}\sin 2\theta_0\\ 0 & -\frac{1}{3} & 0\\ \frac{1}{2}\sin 2\theta_0 & 0 & \sin^2\theta_0-\frac{1}{3}\end{bmatrix}+\frac{\mathbf{I}}{3}. \quad (5)$$

Given the imposed boundary condition $v_x(y=\pm\frac{1}{2},t)=\pm Er\cos\omega t$, the small amplitude oscillatory shear flow limit in this case is the small Ericksen number limit, and so the appropriate solution ansatz for the five independent components of $\mathbf{M}$, flow velocity, and shear stress is to expand around the no-flow equilibrium $\mathbf{M}_0$ **as**

$$\begin{array}{rclrcl} M_{11} &=& \frac{1-s_0}{3}+s_0\cos^2\theta_0+\sum_{k=1}^{\infty}Er^kM_{11}^{(k)}(y,t), & M_{12} &=& 0+\sum_{k=1}^{\infty}Er^kM_{12}^{(k)}(y,t),\\ M_{22} &=& \frac{1-s_0}{3}+\sum_{k=1}^{\infty}Er^kM_{22}^{(k)}(y,t), & M_{23} &=& 0+\sum_{k=1}^{\infty}Er^kM_{23}^{(k)}(y,t),\\ M_{13} &=& \frac{s_0}{2}\sin 2\theta_0+\sum_{k=1}^{\infty}Er^kM_{13}^{(k)}(y,t), & v_x &=& 0+\sum_{k=1}^{\infty}Er^kv_x^{(k)}(y,t),\\ \tau_{12} &=& 0+\sum_{k=1}^{\infty}Er^k\tau_{12}^{(k)}(t). & & & \end{array} \quad (6)$$

At $O(Er)$, the system of the six unknowns $M_{11}^{(1)}, M_{22}^{(1)}, M_{12}^{(1)}, M_{13}^{(1)}, M_{23}^{(1)}$, and $v_x^{(1)}$ block diagonalizes into two systems of three unknowns. The linear system for $M_{11}^{(1)}, M_{22}^{(1)}$, and $M_{13}^{(1)}$ has zero boundary conditions, and so we have the trivial solutions

$$M_{11}^{(1)}(y,t)\equiv 0, \quad M_{22}^{(1)}(y,t)\equiv 0, \quad M_{13}^{(1)}(y,t)\equiv 0. \quad (7)$$

The second system for $M_{12}^{(1)}$, $M_{23}^{(1)}$, and $v_x^{(1)}$ is

$$\begin{aligned} \frac{\partial M_{12}^{(1)}}{\partial t} &= B_1M_{12}^{(1)}+B_2M_{23}^{(1)}+B_3\frac{\partial^2M_{12}^{(1)}}{\partial y^2}+B_4\frac{\partial^2M_{23}^{(1)}}{\partial y^2}+B_5\frac{\partial v_x^{(1)}}{\partial y},\\ \frac{\partial M_{23}^{(1)}}{\partial t} &= B_2M_{12}^{(1)}+B_6M_{23}^{(1)}+B_4\frac{\partial^2M_{12}^{(1)}}{\partial y^2}+B_7\frac{\partial^2M_{23}^{(1)}}{\partial y^2}+B_8\frac{\partial v_x^{(1)}}{\partial y},\\ \tau_{12}^{(1)} &= -\frac{a}{2s_0^2}\left[B_1M_{12}^{(1)}+B_2M_{23}^{(1)}\right]-\frac{1}{s_0^2}\left[B_5\frac{\partial^2M_{12}^{(1)}}{\partial y^2}+B_8\frac{\partial^2M_{23}^{(1)}}{\partial y^2}\right]+B_9\frac{\partial v_x^{(1)}}{\partial y}, \end{aligned} \quad (8)$$

where

$$\begin{aligned} B_1 &= -3\alpha N s_0(1-\cos 2\theta_0), \quad B_2=3\alpha N s_0\sin 2\theta_0, \quad B_3=\frac{2(1-s_0)}{3}+s_0\cos^2\theta_0,\\ B_4 &= \frac{s_0}{2}\sin 2\theta_0, \quad B_5=\frac{a(1-s_0)}{3}+\frac{(a-1)s_0}{2}\cos^2\theta_0, \quad B_6=-3\alpha N s_0(1+\cos 2\theta_0),\\ B_7 &= \frac{2+s_0}{3}-s_0\cos^2\theta_0, \quad B_8=\frac{(a-1)s_0}{4}\sin 2\theta_0, \quad B_9=\mu_1(\frac{1-s_0}{3}+\frac{s_0}{2}\cos^2\theta_0)+\frac{\mu_3}{2}, \end{aligned} \quad (9)$$

subject to the boundary conditions

$$M_{12}^{(1)}(y=\pm\tfrac{1}{2},t)=M_{23}^{(1)}(y=\pm\tfrac{1}{2},t)=0, \quad v_x^{(1)}(y=\pm\tfrac{1}{2},t)=\pm\cos\omega t. \quad (10)$$

The phased-locked solution of the system (8) can be found numerically, and we can use components of the shear stress $\tau_{12}^{(1)}=\tau_1\cos\omega t+\tau_2\sin\omega t$, to express the storage and loss moduli as

$$G'(\omega)=\tfrac{\omega}{2}\tau_2, \quad G''(\omega)=\tfrac{\omega}{2}\tau_1. \quad (11)$$

With the exception of vorticity-aligned anchoring $\theta_0 = \frac{\pi}{2}$, which we address below, we can also use the solution to express the leading order terms of the spectral components as

$$\begin{aligned} s^{(1)} &= \tfrac{1}{2}\beta^{(1)} = -\sin\theta_0 M_{12}^{(1)} + \cos\theta_0 M_{23}^{(1)} \\ \psi^{(1)} &= \tfrac{1}{s_0}(M_{12}^{(1)} + \tan\theta_0 M_{23}^{(1)}), \quad \theta^{(1)} = 0. \end{aligned} \tag{12}$$

Due to the degeneracy of the equilibrium, the third director angle χ does not appear in the spectral representation of either the equilibrium tensor $\mathbf{M}_0$ or the first-order tensor $\mathbf{M}^{(1)}$. However, a first-order solvability condition determines its equilibrium value $\chi_0 = \frac{\pi}{4}$, as in [Forest et al., 2003].

Alternatively, when $\theta_0 \neq \frac{\pi}{2}$, we can recast the system (8) in terms of the more physically relevant spectral quantities (12) as

$$\begin{aligned} \tfrac{\partial \beta^{(1)}}{\partial t} &= A_1\beta^{(1)} + A_2\tfrac{\partial^2\beta^{(1)}}{\partial y^2} + A_3\tfrac{\partial v_x^{(1)}}{\partial y}, \\ \tfrac{\partial \psi^{(1)}}{\partial t} &= A_4\tfrac{\partial^2\psi^{(1)}}{\partial y^2} + A_5\tfrac{\partial v_x^{(1)}}{\partial y}, \\ \tau_{12}^{(1)} &= \tfrac{a}{4s_0^2}\sin\theta_0\Big[A_1\beta^{(1)} + A_2\tfrac{\partial^2\beta^{(1)}}{\partial y^2}\Big] + A_6\tfrac{\partial^2\psi^{(1)}}{\partial y^2} + B_9\tfrac{\partial v_x^{(1)}}{\partial y}, \end{aligned} \tag{13}$$

where $A_1 = -6\alpha N s_0$, $A_2 = \frac{2(1-s_0)}{3}$, $A_3 = -\frac{2a(1-s_0)}{3}\sin\theta_0$, $A_4 = \frac{2+s_0}{3}$, $A_5 = -\frac{1-\lambda_L}{2}$, $A_6 = \frac{1-\lambda_L}{2}\cos^2\theta_0$, for the Leslie tumbling parameter $\lambda_L = \frac{a(2+s_0)}{3s_0}$. In this form, we see a separation into an order parameter equation and a director angle equation linked together by the velocity and shear stress.

3 Exactly solvable cases

There are two limiting cases in which the system (8) can be solved analytically: If $\theta_0 = 0$, the director is aligned with the flow, and if $\theta_0 = \frac{\pi}{2}$, the director is vorticity-aligned. Additionally, there are two simplified versions of the model which can be useful for describing the qualitative behavior of the full system. In the monodomain case, there are assumed to be no spatial gradients in the orientation, and in the Leslie-Ericksen model, the orientation is assumed to be uniaxial with constant order parameters. For flow-aligned anchoring, the order parameters are zero at leading order so that the Leslie-Ericksen model is exact in this case. The authors have previous examined this case in [Choate et al., 2008, 2010].

3.1 Vorticity-aligned anchoring

When $\theta_0 = \frac{\pi}{2}$, $B_2 = B_4 = B_6 = B_8 = 0$, and this decouples one of the three equations in (8) from the other two:

$$\tfrac{\partial M_{23}^{(1)}}{\partial t} = B_7\tfrac{\partial^2 M_{23}^{(1)}}{\partial y^2}. \tag{14}$$

The boundary conditions $M_{23}(y=\pm\frac{1}{2},t)=0$ give the phased-locked solution $M_{23}(y,t)\equiv 0$. The remaining two equations simplify to

$$\begin{aligned}\frac{\partial M_{12}^{(1)}}{\partial t} &= B_1 M_{12}^{(1)} + B_3\frac{\partial^2 M_{12}^{(1)}}{\partial y^2} + B_5\frac{\partial v_x^{(1)}}{\partial y},\\ \tau_{12}^{(1)} &= -\frac{a}{2s_0^2}\left[B_1 M_{12}^{(1)} + B_3\frac{\partial^2 M_{12}^{(1)}}{\partial y^2}\right] + B_9\frac{\partial v_x^{(1)}}{\partial y},\end{aligned} \tag{15}$$

The imposed velocity boundary condition $v_x^{(1)}(y=\pm\frac{1}{2},t)=\pm\cos\omega t$ suggests that we look for phased-locked solutions of the form

$$M_{12}^{(1)}(y,t) = m_1(y)\cos\omega t + m_2(y)\sin\omega t, \quad v_x^{(1)}(y,t) = v_1(y)\cos\omega t + v_2(y)\sin\omega t. \tag{16}$$

We find that

$$\begin{aligned}m_1(y) &= C_1\cosh r_1 y\cos r_2 y + C_2\sinh r_1 y\sin r_2 y + H_1\\ m_2(y) &= C_2\cosh r_1 y\cos r_2 y - C_1\sinh r_1 y\sin r_2 y + H_2,\\ v_1(y) &= F\Big[(C_1 r_1 - C_2 r_2)\cosh r_1 y\sin r_2 y - (C_1 r_2 + C_2 r_1)\sinh r_1 y\cos r_2 y\Big]\\ &\quad -\frac{1}{B_5}\Big(B_1 H_1 - \omega H_2\Big)y,\\ v_2(y) &= F\Big[(C_1 r_2 + C_2 r_1)\cosh r_1 y\sin r_2 y + (C_1 r_1 - C_2 r_2)\sinh r_1 y\cos r_2 y\Big]\\ &\quad -\frac{1}{B_5}\Big(\omega H_1 + B_1 H_2\Big)y,\end{aligned} \tag{17}$$

where $r_1=\sqrt{\frac{-E+\sqrt{E^2+\omega^2}}{2B_3D}}$, $r_2=\sqrt{\frac{E+\sqrt{E^2+\omega^2}}{2B_3D}}$, $D=1+\frac{aB_5}{2B_9s_0^2}$, $E=B_1D$, $F=\frac{B_3(1-D)\omega}{B_5\sqrt{E^2+\omega^2}}$, $H_1=-\frac{B_5(E\tau_1+\omega\tau_2)}{B_9(E^2+\omega^2)}$, $H_2=\frac{B_5(\omega\tau_1-E\tau_2)}{B_9(E^2+\omega^2)}$, $C_1=-\frac{2}{K_3}(H_1\cosh\frac{r_1}{2}\cos\frac{r_2}{2}-H_2\sinh\frac{r_1}{2}\sin\frac{r_2}{2})$, and $C_2=-\frac{2}{K_3}(H_1\sinh\frac{r_1}{2}\sin\frac{r_2}{2}+H_2\cosh\frac{r_1}{2}\cos\frac{r_2}{2})$, where the components of the shear stress and the dynamic moduli are given by

$$\begin{aligned}G'(\omega) &= \tfrac{\omega}{2}\tau_2 = \tfrac{4B_9K_3\omega(\omega K_2 - EK_1 - (E-B_1)K_3\omega)}{4K_3(\omega^2+B_1^2+\omega K_1+EK_1)+K_1^2+K_2^2},\\ G''(\omega) &= \tfrac{\omega}{2}\tau_1 = \tfrac{4B_9K_3\omega(\omega K_1+EK_2+(\omega^2+EB_1)K_3)}{4K_3(\omega^2+B_1^2+\omega K_1+EK_1)+K_1^2+K_2^2},\end{aligned} \tag{18}$$

where $K_1=4FB_5(r_1\sinh r_1+r_2\sin r_2)$, $K_2=4FB_5(r_1\sin r_2-r_2\sinh r_1)$, and $K_3=\cosh r_1+\cos r_2$.

The order parameters in the vorticity anchoring case are still described by (12) so that $s^{(1)}=\frac{1}{2}\beta^{(1)}=-M_{12}^{(1)}$. The leading order terms of the director angles, however, cannot be determined from the $O(Er)$ equations and do not appear in the leading order tensor $\mathbf{M}^{(1)}$ so that the director frame is constant.

3.2 Monodomain problem

The monodomain limit can be solved analytically for any value of θ_0. First, we assume there are no spatial gradients in the orientational variables and impose the velocity $v_x^{(1)}(y,t)=$

$2y\cos\omega t$. Thus, the order parameter equation in (13) decouples, and the biaxiality is

$$\beta^{(1)}(t) = -\frac{8a\alpha N s_0(1-s0)\sin\theta_0}{\omega^2+36\alpha^2N^2s_0^2}\cos\omega t - \frac{4\omega a(1-s_0)\sin\theta_0}{3(\omega^2+36\alpha^2N^2s_0^2)}\sin\omega t. \tag{19}$$

From (12), $s^{(1)} = \frac{1}{2}\beta^{(1)}$. The director angle is $\psi^{(1)}(t) = -\frac{1-\lambda_L}{2\omega}\sin\omega t$, but it does not contribute to the stress at leading order. From the resulting stress, the monodomain moduli are

$$G'_{MD}(\omega) = \frac{\omega^2a^2\alpha N(1-s_0)\sin^2\theta_0}{s_0(\omega^2+36\alpha^2N^2s_0^2)}, \quad G''_{MD}(\omega) = \omega\Big(B_9 + \frac{6a^2\alpha^2N^2(1-s_0)\sin^2\theta_0}{\omega^2+36\alpha^2N^2s_0^2}\Big). \tag{20}$$

3.3 Leslie-Ericksen simplification

A Leslie-Ericksen system assumes perfect alignment with the major director. We modify this assumption slightly to assume that there are no variations of the order parameters away from a uniaxial nematic solution while still allowing the major director to vary. The true LE-limit of our system is $s_0 = 1$, but from (13), we see that if we ignore the $\frac{\partial\beta^{(1)}}{\partial t}$ equation and the contributions to the stress from $\beta^{(1)}$, the remaining equations for $\psi^{(1)}$ and $v_x^{(1)}$ take the same general form as a LE system. This system can be solved in a manner similar to the one studied in [Choate et al., 2008] and predicts the moduli to be

$$\begin{aligned} G'_{LE}(\omega) &= \frac{-A_5A_6B_9^2r\omega^2(\sinh r-\sin r)}{(8A_5^2A_6^2r^2+B_9^2\omega^2)\cosh r-16A_5^2A_6^2r^2\cos r+4A_5A_6B_9r\omega(\sinh r+\sin r)}, \\ G''_{LE}(\omega) &= \frac{B_9^2\omega^2(B_9\omega(\cosh r+\cos r)+2A_5A_6r(\sinh r+\sin r))}{(8A_5^2A_6^2r^2+B_9^2\omega^2)\cosh r-16A_5^2A_6^2r^2\cos r+4A_5A_6B_9r\omega(\sinh r+\sin r)}, \end{aligned} \tag{21}$$

where $r = \sqrt{\frac{B_9\omega}{2(A_4B_9-A_5A_6)}}$.

4 Storage modulus

Figure 1 depicts the storage modulus $G'(\omega)$ for several values of the out-of-plane angle θ_0. For low frequencies, the predictions for all angles increase like $O(\omega^2)$. Flow-aligned anchoring show the largest value while vorticity-aligned has the smallest. However, as ω increases, flow-aligned anchoring changes to $O(\sqrt{\omega})$ growth while vorticity-aligned continues to grow as $O(\omega^2)$ until it surpasses the flow-aligned prediction by two-to-three orders of magnitude. For angles in between, there is a slight plateau before the resumption of $O(\omega^2)$ growth. The plateau is longer for angles closer to flow-aligned. At higher frequencies, the $O(\omega^2)$ growth levels off to an $O(1)$ plateau until at very high frequencies, all angles show $O(\sqrt{\omega})$ growth like flow-aligned.

For a fixed value of ω in the low frequency regime, $G'(\omega)$ is approximately proportional to $\cos^2\theta_0$; however, if ω is in the high frequency regime, $G'(\omega)$ is approximately proportional to $\sin^2\theta_0$. These scalings provide an important guide in the explanation of the two frequency regimes of $G'(\omega)$. We see in (21) that the Leslie-Ericksen storage modulus prediction is directly proportional to $A_6 = \frac{1-\lambda_L}{2}\cos^2\theta_0$, but from (20), the monodomain prediction is directly proportional to $\sin^2\theta_0$. Figure 2 shows graphs of the Leslie-Ericksen and monodomain storage modulus predictions for several values of θ_0.

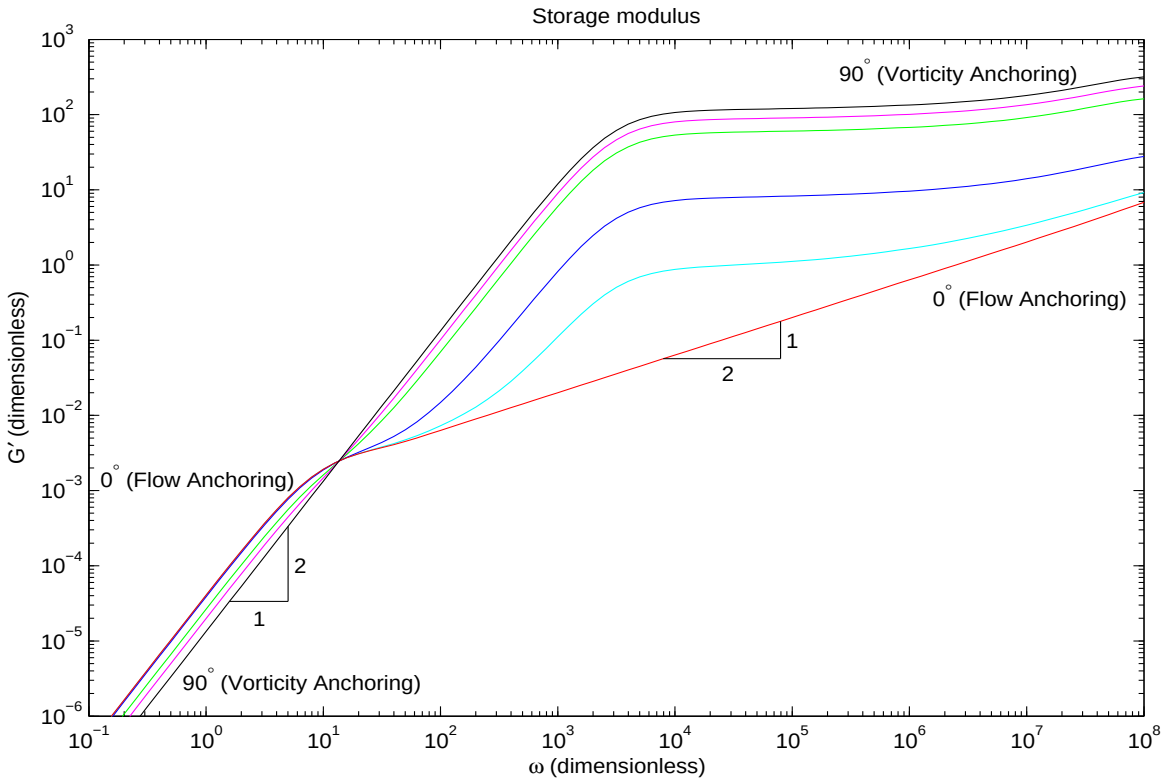

Figure 1: The storage modulus for $\theta_0 = 0°$ (Flow-aligned), 5°, 15°, 45°, 60°, and 90° (Vorticity-aligned)

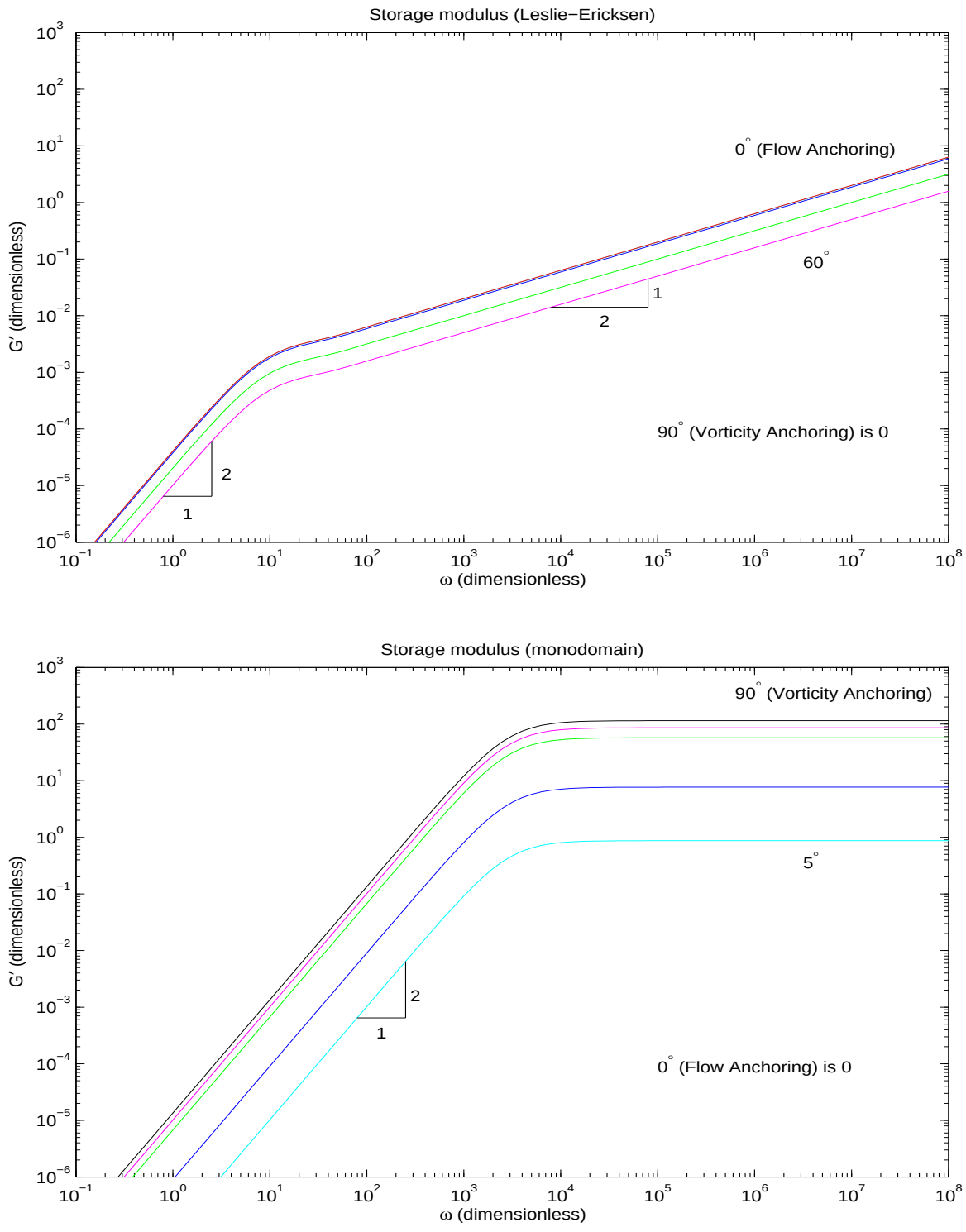

Figure 2: The storage modulus predictions for the Leslie-Ericksen and monodomain models. The Leslie-Ericksen prediction is proportional to $\cos^2\theta_0$ while the monodomain prediction is proportional to $\sin^2\theta_0$.

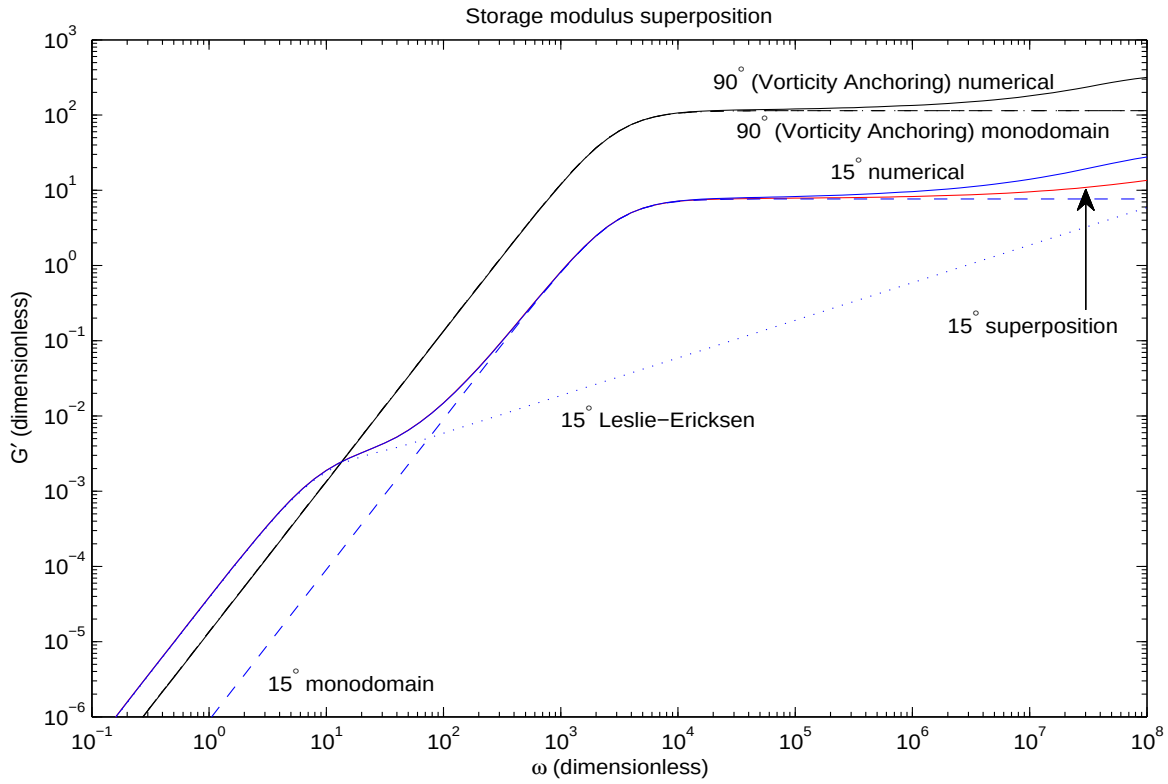

Figure 3: The numerical storage modulus can be well modeled by a simple superposition $G'_{sup} = G'_{MD} + G'_{LE}$.

We can combine these effects with a simple linear superposition

$$G'_{sup} = G'_{MD} + G'_{LE}. \tag{22}$$

Figure 3 compares this superposition with the numerical solution and shows how it effectively captures the transition from the low to high frequency regimes, failing only to quantitatively match the $O(\sqrt{\omega})$ growth for very high frequencies. More importantly, it shows how the out-of-plane angle θ_0 provides a continuous transition between director-dominated behavior and order parameter-dominated behavior. While this occurs for any fixed frequency, it also applies when comparing the high and low frequency regimes. This suggests that low frequency stress is stored in elastic variations of the director whereas higher frequency stress is stored more in deformations of the shape of the orientational distribution rather than its preferred direction. This effect cannot be captured by a Leslie-Ericksen model and requires a tensor model.

5 Viscosity

Since the loss modulus $G''(\omega)$ is mostly linear with the frequency ω, it is easier to analyze by examining the viscosity $\eta'(\omega) = \frac{G''(\omega)}{\omega}$. Figure 4 shows the viscosity $\eta'(\omega) = \frac{G''(\omega)}{\omega}$ for several

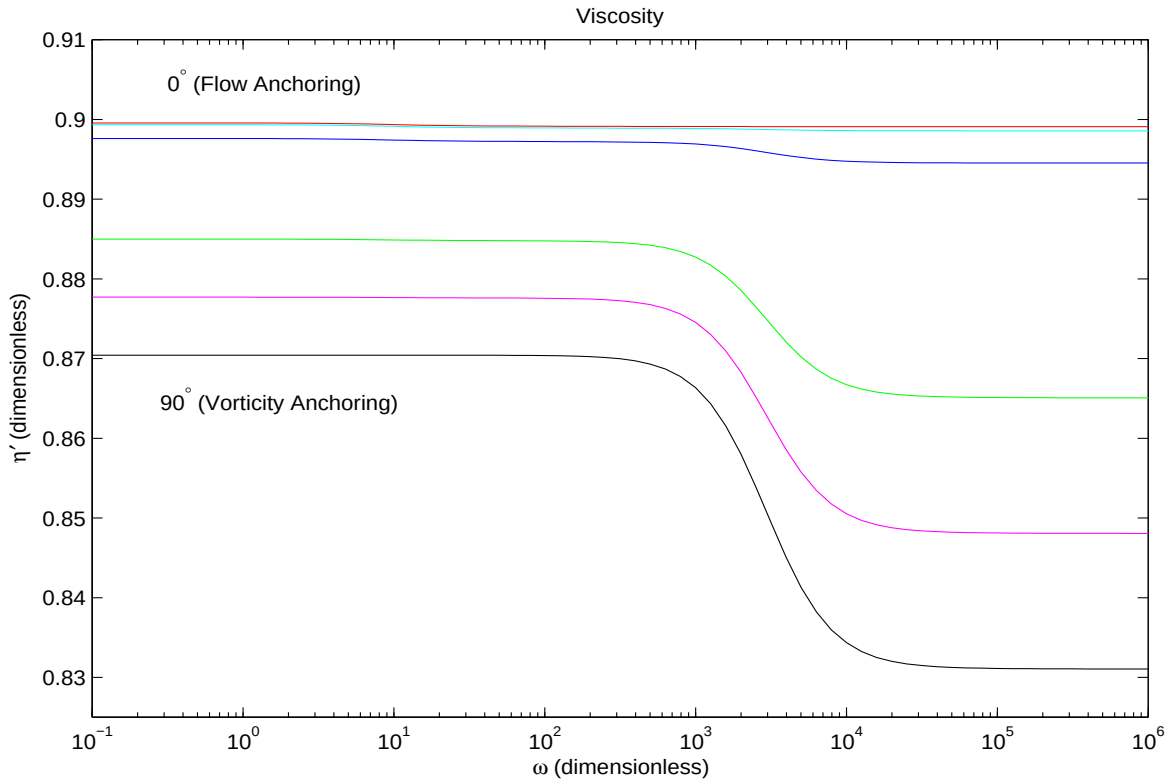

Figure 4: The numerical viscosity for $\theta_0 = 0°$ (Flow-aligned), 5°, 15°, 45°, 60°, and 90° (Vorticity-aligned)

values of θ_0. For all frequencies, η' increases from vorticity-aligned anchoring to flow-aligned. When a rigid spheroidal molecule with aspect ratio R is aligned with its major axis in the shearing plane, its moment of inertia with respect to rotation about the vorticity axis is larger than when the same molecule aligned parallel to the vorticity axis by a factor of $\frac{1+R^2}{2}$. Therefore, it should be expected that vorticity-aligned anchoring has a lower viscosity.

Flow-aligned anchoring shows little frequency dependence with the low frequency values being slightly larger than for high frequencies. For vorticity-aligned anchoring, this thinning at high frequencies is much more pronounced, with the high frequency response being only 90-95 percent as viscous as the low frequency response.

As in the storage modulus, the monodomain and LE models can give us insight into this behavior. In Figure 5, the LE prediction is essentially independent of the frequency, with the small exception of a slight rise for low frequencies for near in-plane angles, which corresponds nicely with that found in the numerical predictions. The monodomain prediction shows shear thinning at higher frequencies much like the numerical case. From (19), the monodomain order parameters can be rewritten as

$$s^{(1)} = \tfrac{1}{2}\beta^{(1)} = -\frac{2a(1-s_0)\sin\theta_0}{3\sqrt{\omega^2+36\alpha^2N^2s_0^2}}\cos\left(\omega t - \tan^{-1}\frac{\omega}{6\alpha N s_0}\right), \tag{23}$$

Thus, for low frequencies, there is a negative or defocusing contribution to s that is nearly

in phase with the strain rate and therefore contributes to the viscosity because the $A_1\beta^{(1)}$ term in $\tau_{12}^{(1)}$ is (13) is positive. However, as the frequency increases, the magnitude of this defocusing effect decays like $O(\omega^{-1})$, and it shifts out of phase with the strain rate, which decreases the viscosity when compared with the low-frequency regime. The onset of this decay also corresponds to the transition to the plateau seen in $G'(\omega)$. For all frequencies, this defocusing contribution to the viscosity is proportional to $\sin\theta_0$, and therefore it is not seen for flow-aligned anchoring and is maximized by vorticity-aligned anchoring.

We can capture the numerical viscosity quite well with a linear superposition of the monodomain and Leslie-Ericksen predictions

$$\eta'_{sup} = \eta'_{MD} + \eta'_{LE} - B_9. \tag{24}$$

Figure 6 shows this superposition is essentially indistinguishable from the numerical prediction. The reasoning behind this form can be seen by rewriting the shear stress as

$$\begin{aligned} \tau_{12}^{(1)} = \quad & \left[\tfrac{a}{4s_0^2}\sin\theta_0 A_1\beta^{(1)} + 2B_9\cos\omega t\right]_1 - 2B_9\cos\omega t \\ & + \tfrac{a}{4s_0^2}\sin\theta_0 A_2\tfrac{\partial^2\beta^{(1)}}{\partial y^2} + \left[A_6\tfrac{\partial^2\psi^{(1)}}{\partial y^2} + B_9\tfrac{\partial v_x^{(1)}}{\partial y}\right]_2. \end{aligned} \tag{25}$$

The terms in brackets 1 take the same basic form as the monodomain stress, while the terms in brackets 2 take the same form as the Leslie-Ericksen stress.

6 The role of the gap width

We find that the moduli have a similar dependence on the nondimensional gap width parameter $\alpha = \frac{8h^2}{N\mathcal{L}^2}$ as in [Choate et al., 2010]. Since α does not appear in the LE equations, the LE moduli from (21) are independent of α. Both of the monodomain predictions (20), however, depend on α through the relationship

$$G_{MD}(\omega;\alpha) = \alpha G_{MD}(\tfrac{\omega}{\alpha};1). \tag{26}$$

The monodomain viscosity scales as $\eta_{MD}(\omega;\alpha) = \eta_{MD}(\frac{\omega}{\alpha};1)$.

The superposition models (22) and (24) provide a way to scale the numerical predictions as

$$\begin{aligned} \tfrac{G'(\omega;\alpha)-G'_{LE}(\omega)}{\alpha} \quad & \approx G'_{MD}(\tfrac{\omega}{\alpha};1), \\ \eta'(\omega;\alpha) + B_9 - \eta'_{LE}(\omega) \quad & \approx \eta'_{MD}(\tfrac{\omega}{\alpha};1). \end{aligned} \tag{27}$$

Figure 7 shows the numerical storage modulus and viscosity for several values of α for $\theta_0 = 15°$. The inserts show the numerical values rescaled according to (27), and we see that they collapse onto the monodomain prediction in the vicinity of the transition from $O(\omega^2)$ growth to the plateau of G' and the transition to the slightly thinner high-frequency regime in η'.

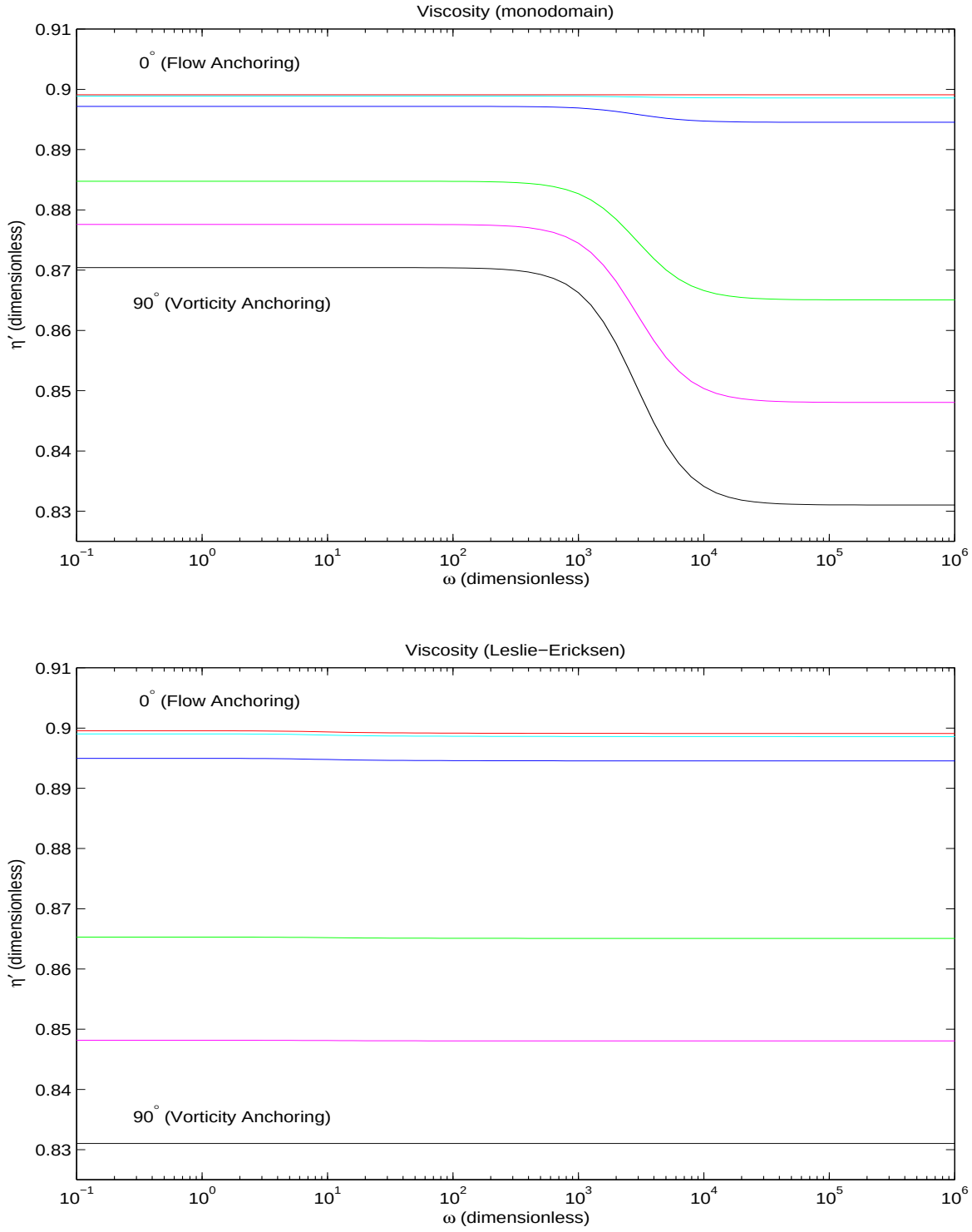

Figure 5: The viscosity predictions for the monodomain and Leslie-Ericksen models.

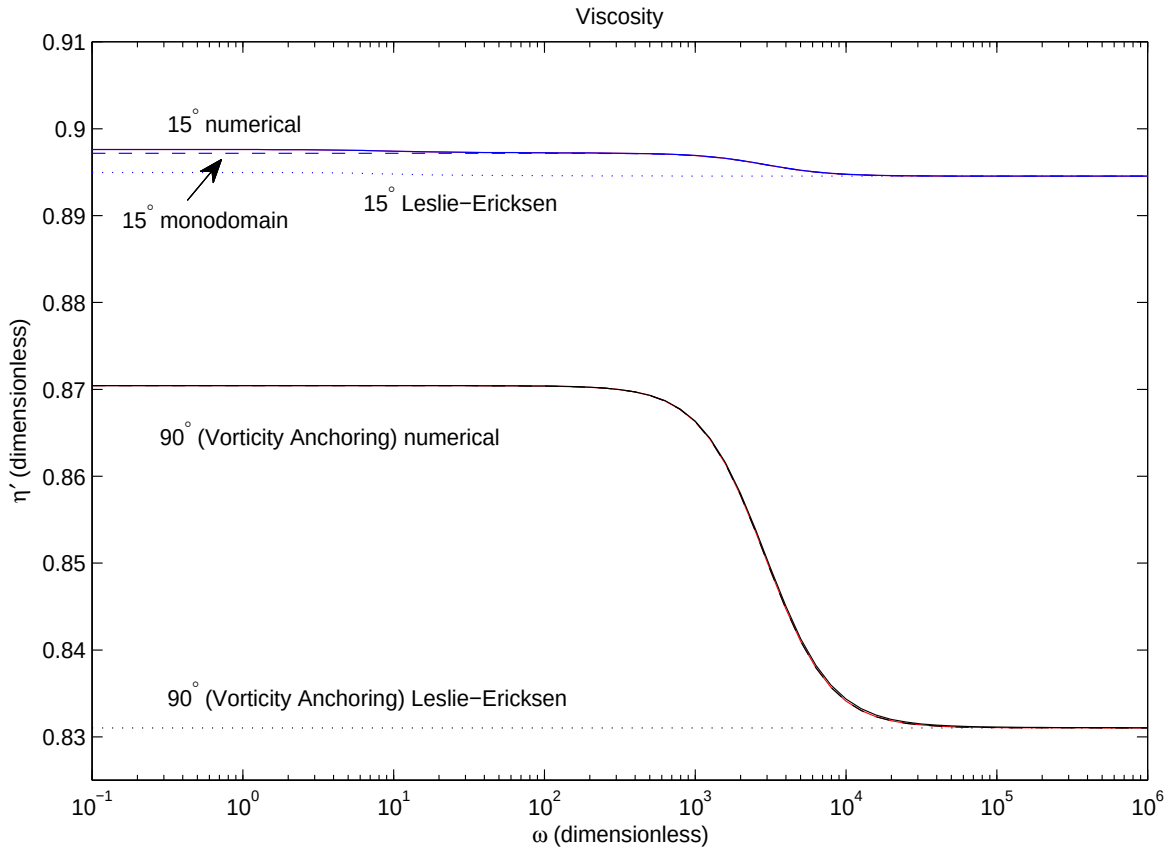

Figure 6: The numerical viscosity can be well modeled by a simple superposition $\eta'_{sup} = \eta'_{MD} + \eta'_{LE} - B_9$.

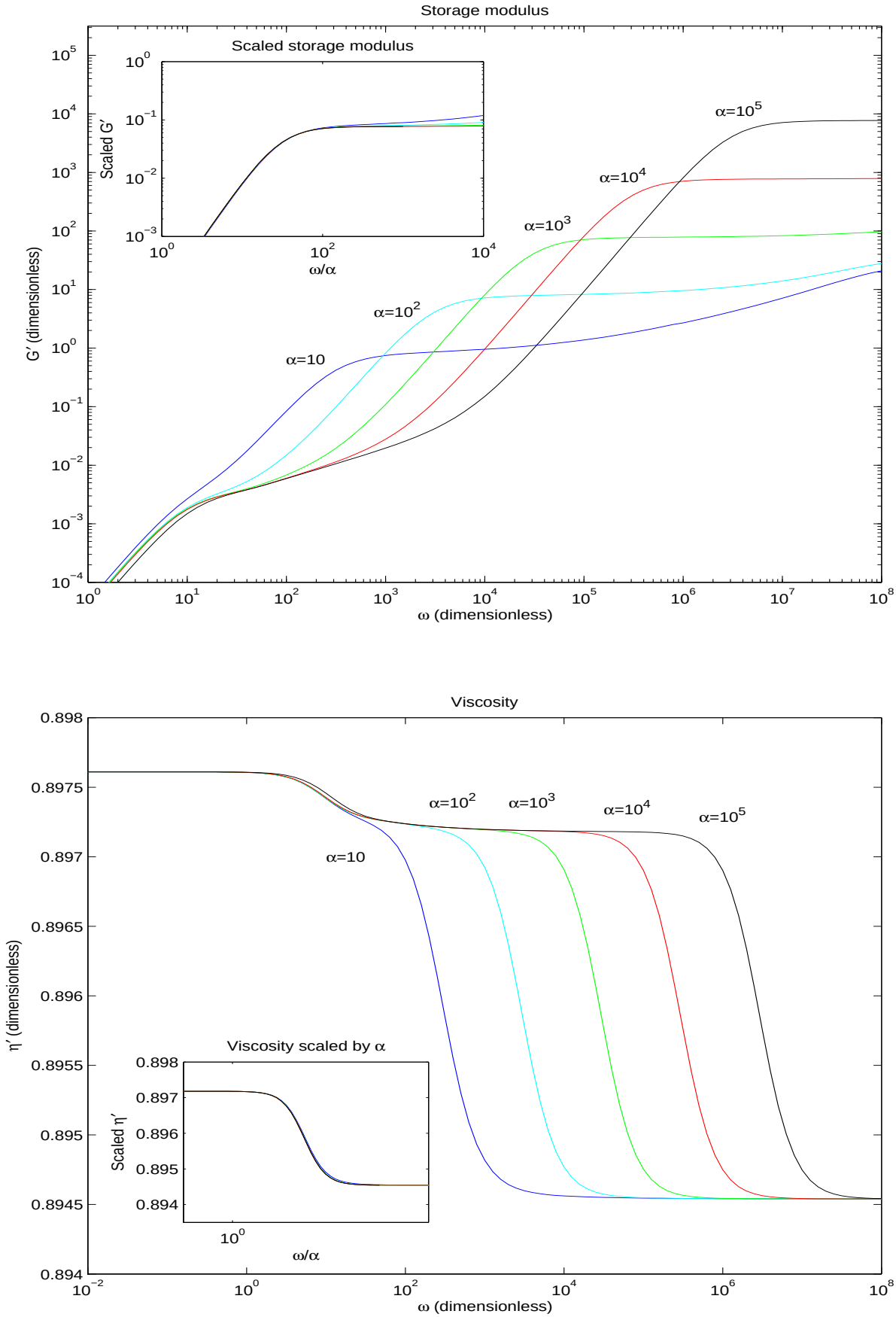

Figure 7: The storage modulus and viscosity for several values of $\alpha = \frac{8h^2}{N\mathcal{L}^2}$ for $\theta_0 = 15°$.

7 Conclusion

We have shown that the dynamic moduli of nematic polymers in small amplitude oscillatory shear can be tuned by rotation of the rubbing axis of the plates relative to the direction of plate motion (the flow direction). The moduli are derived and computed versus the angle θ_0 between the rubbing angle and the direction of the plate motion. We find that the storage moduli are the most sensitive in the high frequency range with up to three orders of magnitude gain in G' when $\theta_0 = \frac{\pi}{2}$ (vorticity-aligned anchoring) compared to 0 (flow-aligned anchoring). These storage moduli phenomena are due to fluctuations and gradients in the order parameters of the orientation tensor, and therefore are not captured by the Leslie-Ericksen theory.

References

de Andrade Lima LRP, Rey AD (2004) Assessing flow alignment of nematic liquid crystals through linear viscoelasticity. Phys Rev E **70**:011701

de Andrade Lima LRP, Rey AD (2006) Superposition principles for small amplitude oscillatory shearing of nematic mesophases. Rheol Acta **45**: 591-600

Burghardt WR (1991) Oscillatory shear flow of nematic liquid crystals. J Rheol **35**: 49-62

Choate EP, Cui Z, Forest MG (2008) Effects of strong anchoring on the dynamic moduli of heterogeneous nematic polymers. Rheol. Acta **47**: 223-236

Choate EP, Forest MG, Ju L (2010) Effects of strong anchoring on the dynamic moduli of heterogeneous nematic polymers II: Oblique anchoring angles. Rheol. Acta **49**: 335-347

Forest MG, Zhou R, Wang Q (2003) Full-tensor alignment criteria for sheared nematic polymers. J. Rheol. 47: 105-127

Holmes CJ, Cornford SL, Sambles JR (2010) Small Surface Pretilt Strikingly Affects the Director Profile during Poiseuille Flow of a Nematic Liquid Crystal. Phys. Rev. Lett. **104**: 248301

Mendil H, Baroni P, Noirez L (2005) Unexpected giant elasticity in side-chain liquid-crystal polymer melts: A new approach for the understanding of shear-induced phase transition. Europhys Lett **76**: 983-989

Mendil H, Baroni P, Noirez L (2006) Solid-like rheological response of non-entangled polymers in the molten state. Euro Phys J E **19**:77-85

Pujolle-Robic C, Noirez L (2001) Observation of shear-induced nematic-isotropic transition in side-chain liquid crystal polymers. Nature **409**: 167-171

Wang Q (2002) A hydrodynamic theory of nematic liquid crystalline polymers of different configurations. J Chem Phys **116**: 9120-9136